Polymer conformations of gas-hydrate kinetic inhibitors: A small-angle neutron scattering study

H. E. King, Jr.,[a] Jeffrey L. Hutter,[b] Min Y. Lin,[c] and Thomas Sun[d]
Exxon Mobil Research and Engineering Company, Annandale, New Jersey 08801

(Received 19 July 1999; accepted 9 November 1999)

We have used small-angle neutron scattering to characterize the polymer conformations of four nonionic water soluble polymers: poly(ethylene oxide), poly(N-vinyl-2-pyrollidone), poly(N-vinyl-2-caprolactam), and an N-methyl, N-vinylacetamide/N-vinyl-2-caprolactam copolymer. The last three of these are able to kinetically suppress hydrate crystallization, and their inhibitor activity ranges from moderate to very effective. This attribute is of significant commercial importance to the oil and gas industry, but the mechanism of the activity is unknown. The dilute-solution polymer conformation in a hydrate-forming tetrahydrofuran/water fluid shows little difference among the four polymers: the majority of the scattering is that expected for a polymer in a good solvent. Each solution also exhibits some additional low-q scattering which we attribute to aggregates. In the presence of a hydrate-crystal/liquid slurry, the three inhibitor polymers significantly change their conformation. Utilizing results from our previous contrast variation study, we show that this arises from polymer adsorbed to the hydrate-crystal surface. Furthermore, we find a strong correlation between the scattering intensity at low q values and the effectiveness of the inhibitor polymer. We suggest this is an indication that as surface adsorption increases, the inhibitor's blocking of growth sites increases. Also measured for one of the kinetic-inhibitor polymers was the dilute-solution polymer conformation in a hydrate-forming propane/water fluid (hydrate crystal free). This system shows additional low-q scattering, possibly indicating a polymer–propane interaction prior to crystal formation. This may affect hydrate nucleation behavior and offer a second mechanism for kinetic hydrate inhibition. © *2000 American Institute of Physics.* [S0021-9606(00)70605-2]

I. INTRODUCTION

Gas hydrates are ice-like crystals consisting of water cages surrounding small molecules such as propane or methane.[1] Enclathration of the small molecules is key to the crystals' stability, and depending upon the gas pressure their melting point can extend to temperatures well above that of ice. Because of this, they crystallize in many settings where ordinary ice is not stable. For example, there are many natural-gas hydrate deposits on the sea floor associated with gas seepage into cold ocean water.[2] Similar conditions can be found in oil and gas transport pipelines. Under deep-sea conditions, inside such pipelines one finds a ready supply of water and natural gas at temperatures of ~5 °C and pressures of ~100 MPa. Thus, hydrate formation within pipelines is a significant long-standing problem for the oil industry.[3] The consequences of hydrate formation can be very serious. Blockage of the pipeline, with consequent temporary loss of production is one scenario, but it is also possible for the pipeline to become permanently blocked or for attempts to release the hydrate plug to cause serious accidents. The solid plug can be released as a ballistic object launched by a high differential pressure. These serious consequences have led to treatments to prevent hydrate formation. In addition to installing thermally insulated pipelines, a common approach has been to add an antifreeze compound, typically methanol, to suppress the formation temperature.[4] Although effective, this approach has drawbacks such as the requirement for high volume fractions of methanol (up to 50 vol%) with the potential environmental impact of spillage. Also, there are considerable costs associated with supply and recovery of the methanol.

As with many other crystallization problems, there is the possibility of kinetic inhibition rather than thermodynamic suppression. Recently it has been found that certain water-soluble polymers can kinetically inhibit hydrate formation.[5] Experiments show that at the low concentrations of use, less than 1 wt%, there is little or no shift in the equilibrium hydrate formation point. But they are able to inhibit hydrate formation by several degrees during continuous cooling and are able to suppress crystallization for long time periods at intermediate levels of subcooling. These laboratory tests were sufficiently promising to encourage tests in actual pipelines, where indications are positive for the polymers' commercial use.[6]

Despite these technical achievements, the mechanism of inhibition remains unclear.[7–9] From the time of their discovery, there has been an ongoing debate as to whether the polymers act on the surface of an already existing crystal or

[a]Author to whom correspondence should be addressed.
[b]Present address: Physics Department, University of Western Ontario, London, ON N6A 5B9, Canada.
[c]Also at the National Institute of Standards and Technology, Gaithersburg, MD 20899.
[d]Present address: Exxon Mobil Chemical Company, Baytown, TX 77522.

whether they associate in some manner with hydrate-forming constituents while still in solution. In a companion article[10] we describe contrast–variation, small-angle neutron scattering (SANS) experiments for one inhibitor polymer, poly (N-vinyl-2-pyrollidone), hereafter PVP, in which we determine the polymer adsorption on the hydrate crystal surface. The measured surface layer is unusual. Rather than forming a uniform layer, the polymer covers only 2% of the total crystal surface. Likely, the polymer forms clumps (local concentration about $2.5c^*$, where c^* is the chain-overlap concentration) on the surface, with each clump having dimensions several times that of the polymer radius of gyration. Associated with the formation of the polymer layer is an increase in the total surface area of the crystals relative to that of crystals prepared in an identical way, but with no inhibitor polymer. Optical studies of crystal growth morphology had already identified a significant alteration of crystal growth morphology associated with the inhibitor polymers: the crystal growth shape changes from octahedral to plate-like.[7,8,11] The increase in surface area measured by the SANS experiments is consistent with this morphology change. If, as expected, the polymer clumps act as growth inhibitors, one expects that the inhibition ability of the polymers rests with their ability to suppress growth at the early crystal-growth stage, before the crystal size and volume in a pipeline exceeds that which would hinder flow. An explanation of the alteration of growth morphology is more complex. Each face of the resulting thin plate is crystallographically equivalent. Therefore, a symmetry breaking, on a macroscopic length scale is necessary. A possible cause is that slight differences in polymer concentration occur on the crystal as it forms, resulting in a differential growth rate which is amplified through an interaction with the surrounding concentration field.[7,8] This is further discussed by Hutter *et al.*[10]

In the preceding work, surface adsorption onto hydrate crystals was shown to be an important attribute of PVP. In the present work we will compare the surface adsorption and solution characteristics of four polymers: poly(ethylene oxide) (hereafter PEO), PVP, poly(N-vinyl-2-caprolactam) (hereafter PVCap), and an N-methyl, N-vinylacetamide/N-vinyl-2-caprolactam copolymer (hereafter VIMA/VCap). These range in inhibitor effectiveness from inactive (PEO) to very active (VIMA/VCap). As we will see, the present work suggests that the polymer adsorption is strongly correlated with the inhibitor's effectiveness. This further strengthens the case for surface activity being an important inhibitor attribute. There is much less to distinguish the solution properties among the four polymers. Each is largely described by a typical ''good solvent'' conformation. This is consistent with light scattering studies of PVP[12] and PVCap[13] in water, and of PVP in water/tetrahydrofuran mixtures.[14] However, each polymer also exhibits some excess low-q scattering. This may be due to polymer aggregation, which is often reported for water-soluble polymers. We discuss these features below.

The majority of the experiments discussed here were conducted with a water-soluble hydrate forming molecule, tetrahydrofuran (hereafter THF). However, naturally-forming hydrates are composed of gaseous hydrocarbons, solubilized in water only through application of elevated pressure. Therefore, we also present results on a system of PVP in D_2O under elevated propane gas pressure. In these experiments, we supercool the solution well into the hydrate stability regime without forming hydrate crystals. This allows us to examine the polymer's conformation, which we find to be unchanged as we pass into the hydrate forming region. However, we note that there is excess scattering at small q values, indicating a supramolecular structure. We discuss possible origins for this behavior.

II. EXPERIMENT

A. Sample preparation

The structure II hydrate crystal studied here has a cubic lattice with edge length $a=17.24$ Å and an idealized formula $X\cdot 17H_2O$, where X is an enclathrated molecule. We utilize X=tetrahydrofuran for the majority of our work. Tetrahydrofuran, being water soluble, assures uniform hydrate formation throughout the sample. We also used X=propane, where a fixed propane pressure was applied to a water sample allowing us to move in and out of the hydrate-stable region of the phase diagram by varying temperature. In all of these samples, D_2O replaced H_2O to minimize the incoherent neutron scattering. The influence of D_2O on the hydrate phase diagram has been measured by Hanley *et al.*[15] and is discussed by Hutter *et al.*[10] The overall effect is to elevate the melting temperatures of the crystalline phases: both the ice and hydrate melting points are elevated by about 3 °C.

For the D_2O/THF experiments, we created partially frozen slurries consisting of hydrate crystals and THF-depleted solution. To do this, we prepared samples with a 1:25 mole ratio of deuterated THF (hereafter TDF) to D_2O water. The solvents utilized were D_2O:DLM-4 grade, 99.9 at.% enrichment. Cambridge Isotope Laboratories and TDF: tetrahydrofuran-d_8 99.5 at.% enrichment. Aldrich. Each of our four different polymers (described in Table I) was added to this solvent at approximately 0.5 wt%. The relevant neutron scattering length densities are given in Table II.

Once prepared, each solution was transferred to a standard quartz banjo cell 0.5 cm thick and 2 cm in diameter. To each cell we added a magnetic stir bar to allow agitation during crystallization. For crystal-plus-liquid slurry formation, cooling to the desired temperature in a water bath produced partially frozen samples. Often, we needed to nucleate the hydrate phase by locally cooling the sample with a cold point. Continuous stirring during the freezing process results in a roughly uniform distribution of crystals (approximately 40 μm across as measured by optical microscopy) surrounded by the TDF-depleted solution. The samples were transferred to a controlled temperature stage mounted on the beamline and held at constant temperature during the neutron scattering runs. For experiments in the fully liquid state, we used a temperature of 7 °C, and for the liquid-plus-crystal slurry samples, we used temperatures from 2.5 °C to 3.5 °C. Examination of the D_2O-THF phase diagram indicates a volume fraction of solid of approximately 0.5 at those temperatures as shown in Fig. 1 of Hutter *et al.*[10] Furthermore, due to the relative insensitivity of the liquidus line to composi-

TABLE I. Polymers used in this study.

Polymer	Acronym	Source	Monomer weight (g/mol)	Molecular weight (g/mol)	M_W/M_N	A_2 (ml mol/g^2)[a]	Concentration (g/cc)	Concentration (volume fraction)
Polyethylene oxide	PEO	TOSOH Corporation Tokyo, Japan. SE-5, (Batch RE-23)	44.0532	46 000	1.1	2.15×10^{-3}	0.005 53	0.004 91
Poly(N-vinyl-2-pyrollidone)	PVP	see Sun and King[b]	111.1436	49 000	3.2	8.40×10^{-4}	0.005 54	0.004 38
Poly(N-vinyl-1-2-caprolactam)	PVCap	synthesized in house	139.1974	113 000[c]	···	1.83×10^{-4}	0.006 79	0.005 37
N-methyl, N-vinylacetamide/ N-vinyl-2-caprolactam (1:1) copolymer	VIMA/VCap	synthesized in house	238.3300	29.200	···	d	0.005 23	0.004 13

[a]Values calculated utilizing data as follows: PEO (Ref. 25); PVP (Ref. 12); PVCap (Ref. 13).
[b]Reference 12.
[c]Molecular weight calculated from Guinier amplitude.
[d]Value unavailable, assumed zero in calculations.

tion at these conditions, small fluctuations of temperature have little effect on the solid/liquid ratio. We examined the polymers in the liquid-state samples both before and after freezing and found no significant differences.

The objective for the D_2O propane experiments was to examine the polymer conformation of a hydrate-inhibitor polymer in a solvent saturated with a hydrate-forming gas. Using a D_2O-filled variable-temperature, pressure cell[16] mounted on the beamline, we monitored the polymer conformation at temperatures of 20 °C, 10 °C, 6.7 °C, and 3.7 °C and a gas pressure of 655 kPa. This probes conditions above and below the hydrate formation line.[17] From the work of Kobayashi and Katz,[18] the propane content of the water along this isobar can be estimated to range from about 0.000 15 to 0.0004 mole fraction of propane. As expected, due to the nucleation barrier, no hydrates formed at these subcoolings over the course of the neutron scattering runs.

B. Data collection and reduction procedure

The small angle neutron scattering measurements were performed at the NIST Center for Neutron Research, in Gaithersburg, MD. Two SANS instruments, NG3 and NG7, which are almost identical, were utilized. We chose a suitable range of momentum transfer of $0.002<q<0.2$ Å within the instrument capabilities, where $q=4\pi\sin(\theta/2)/\lambda$ (θ is the scattering angle and λ the neutron wavelength). This was accomplished in two configurations (low-q and high-q) with a common wavelength, $\lambda=7$ Å. Each covers about 1.2 decades of q, with a significant overlap between the low-q and high-q configurations. The scattering intensities were reduced to differential scattering cross-section $d\Sigma/d\Omega$ using the standard techniques of subtracting the contributions from the empty cell and other background and referencing to a known standard. The scattered intensity was measured by a

TABLE II. Neutron scattering lengths for components studied.

Material	Composition	Molecular weight (g/mol)	Density (g/cm^3)	Scattering length density[a] ($\times10^{10}$ cm^{-2})
D_2O/TDF solvent	$D_2O_{0.9616}\cdot(C_4D_8O)_{0.039\,93}$	22.333[b]	1.111[c]	6.493
TDF-depleted solvent[d]	$D_2O_{0.97762}\cdot(C_4D_8O)_{0.022\,89}$	21.370[b]	1.113[c]	6.467
Hydrate crystal	$17D_2O\cdot(C_4D_8O)_{0.999}$	420.467[b]	1.090	6.410
PEO	$(C_2H_4O)_n$	44.0532	1.126	0.637
PVP	$(C_6H_9ON)_n$	111.1436	1.264[e]	1.460
PVCap	$(C_8H_{13}ON)_n$	139.1974	f	1.075
VIMA/VCap (1:1)	$(C_{13}H_{22}O_2N_2)_n$	238.3300	f	1.097

[a]Using values from Lovesey (Ref. 34).
[b]Assuming 99.9% deuteration for D_2O and 99.5% deuteration for TDF.
[c]Using densities and the excess volume of mixing from Kiyohara and Benson (Ref. 35), with an empirical correction factor determined in Hutter *et al.* (Ref. 10). TDF density obtianed through TDF/THF molecular weight ratio.
[d]Assuming a mole fraction of 0.488 D_2O freezing into hydrate crystals [see Hutter *et al.* (Ref. 10)].
[e]Effective density in aqueous phase (Ref. 36).
[f]Density assumed equal to that for PVP for calculations.

two-dimensional area detector. The intensities were symmetric about the beam center (with the exception of some slurry samples, as discussed below). Thus, we averaged the data radially to obtain $d\Sigma/d\Omega$ as a function of q. The precise procedure for obtaining and reducing data is documented in the NIST SANS Data Acquisition and Reduction manuals.[19] The data acquisition procedure includes two types of measurements, as described below.

The transmission measurements determine the transmitted intensity for each sample. These measure the intensity at $q=0$ (as opposed to the scattered intensity, $q>0$), so are always measured at the low-q configuration. Transmission measurements require the following runs. (i) An empty position run with no sample present (i.e., an empty sample slot). An attenuator is used to prevent detector damage from the direct beam at $q=0$. (ii) Step (i) is repeated for each sample, either at the same slot, or at a similar slot in a multiple sample-changer. (iii) Step (ii) is repeated for an empty cell. (iv) Step (ii) is repeated for a standard sample. The transmission factors for the sample (Tsam), cell (Tcell), and the standard (Tstd), are determined as the ratio between the total counts in a central region near $q=0$ from runs (ii) to (iv), respectively, to the corresponding counts in the same region of run (i). We use a square region, 8 pixels per side, that is completely illuminated by the direct beam. Because each step will only result in one number (the transmission factor), the measurement time is quite minimal, usually 2 min for each run.

The scattering measurements ($q>0$) consisted of the following steps, and consumed the bulk of our experiment time because each measurement contains data points over a wide range of q-values and the scattered intensity is much weaker than the incident intensity. In these runs, the attenuator is removed to provide the highest possible neutron flux. Instead, a beam stop slightly larger than the direct beam is placed in the center to prevent the region from being damaged by the direct beam. The following runs are performed. (v) In the sample slot, a neutron absorber (Li glass) is placed to stop the neutron beam at the sample position. This allows the detector to measure the overall background both due to other neutron sources, and detector dark current which is unrelated to measured samples or cells. (vi) Step (v) is repeated for each sample at the same slot, or at a similar slot with the sample-changer. (vii) Step (vi) is repeated for the empty cell. (viii) Step (vi) is repeated for the standard sample. Each step takes about 2 to 3 h for the low-q, low flux configuration, and 20 to 30 min for the high-q high flux configuration, depending on how strong the scattering intensity is for each sample.

The data reduction procedure is as follows. (a) Obtain transmission factors as already described. (b) The background and empty cell contributions to the scattering of each sample are subtracted according to the prescription,

$$\begin{aligned}&\text{corrected scattering}\\&=[\text{run(vi)}-\text{run(v)}]-[\text{Tsam/Tcell}]\\&\quad\times[\text{run(vii)}-\text{run(v)}].\end{aligned}\tag{1}$$

The scaling factor [Tsam/Tcell] takes into account the difference in attenuation between run (vi) and run (vii) in order not to over-subtract the cell contribution.[20] (c) The corrected 2D data from (b) is divided pixel-by-pixel by a 2D detector efficiency correction. This is periodically measured using an isotropic scatterer such as water. (d) The 2D data are related to the absolute scattering cross-section $d\Sigma(q)/d\Omega$ according to

$$I(q)=\Phi A d\,\text{Tsam}\,\frac{d\Sigma(q)}{d\Omega}\Delta\Omega\epsilon t,\tag{2}$$

where Φ is the neutron flux on the sample, A the sample area, d the sample thickness, $\Delta\Omega$ the solid angle subtended by one detector pixel, ϵ the detector efficiency, and t the integration time. By dividing this expression by a similar one measured for a known standard sample [run (viii) going through the same procedure (a) to (c)], we can solve for the absolute scattering cross-section for the samples

$$\frac{d\Sigma(q)}{d\Omega}=\frac{I(q)}{I_{\text{std}}(0)}\,\frac{d_{\text{std}}}{d}\,\frac{\text{Tstd}}{\text{Tsam}}\,\frac{d\Sigma_{\text{std}}(0)}{d\Omega},\tag{3}$$

where $I_{\text{std}}(0)$ is the measured scattering from the standard, extrapolated to $q=0$, d_{std} is the thickness of the standard, and $d\Sigma_{\text{std}}(0)/d\Omega$ is the reference value for the absolute scattering cross-section of the standard at $q=0$. (e) $d\Sigma(q)/d\Omega$ is determined by radially averaging the 2D data (after masking out those pixels which are known to be inaccurate).

We followed a similar procedure with the pressure cell. Empty cell runs were performed with no solvent in the cell and the effectiveness of the subtraction was checked by examining the q-dependence of scattering from D_2O enclosed within the cell.

C. Neutron scattering contrast calculations

The measured scattering, $d\Sigma(q)/d\Omega$, can be expressed as the sum of terms, each of which is the product of a structure factor that describes a particular structure in the sample and the contrast corresponding to that term. We determine the contrasts from the scattering length densities n_α of each component α in the system. In general n_α is calculated as the total molecular scattering length of component α divided by its volume V_α:

$$n_\alpha=\frac{1}{V_\alpha}\sum_{\text{molecules}} b_i,\tag{4}$$

where b_i is the scattering length of the ith molecule. Thus, knowing the composition and density of each component, we can calculate its scattering length density. Values for the samples in this study are recorded in Table II. The contrast factors then depend on the differences in scattering length densities between components. Note that the contrast between solvent and hydrate is inherently small since both have similar composition, but that the contrasts between solvent and the (undeuterated) polymers are relatively large. This feature is advantageous in detecting even small amounts of polymer on the crystal surface.

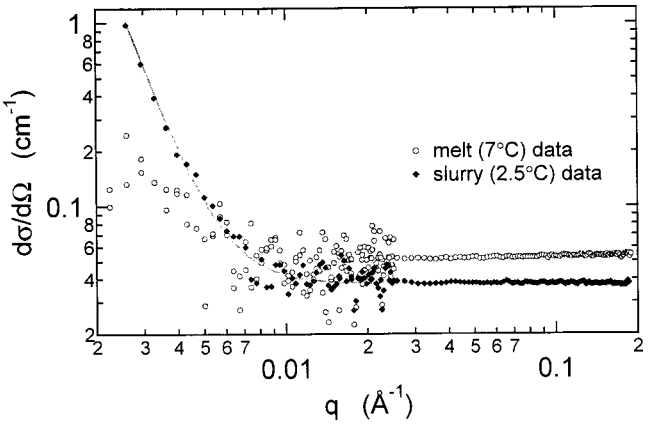

FIG. 1. Differential scattering cross-section for TDF/D_2O solvent. At 7 °C, the scattering from the completely melted solvent is essentially isotropic. At 2.5 °C, the sample is partially frozen. The solid line is a best fit to the Porod scattering, Eq. (5), including a q-independent background term.

III. RESULTS

A. Polymer-free solution and slurry

Data for the solvent (1:25 TDF in D_2O) with no added polymer are shown in Fig. 1. The sample is liquid at 7 °C, resulting in essentially isotropic scattering from thermally-activated density fluctuations (of course, there is a peak in the liquid structure-factor, but this cannot be seen at the low q-values probed here). The small intensity rise at low q may be due to particles in the solution or to imperfect subtraction of the empty-cell scattering; in any event, it is considerably less than the signal of interest. At 2.5 °C, the data show a significant low-q signal. This Porod scattering is from the crystal–liquid interfaces in the partially frozen sample.

The Porod scattering is given by [see Eq. (8.31) from Higgins and Benoît][20]

$$I_{\text{Porod}}(q) = 2\pi(n_h - n_s)^2 (S/V) q^{-4}, \tag{5}$$

where n_h is the scattering length density of the hydrate crystal, n_s is that of the surrounding fluid, and S/V is the interfacial surface area per unit scattering volume (provided that $q \gg 1/R$, where R is the radius of curvature of the surface—a good assumption for our faceted crystals). Thus, the Porod scattering provides a measure of the surface area present; for this polymer-free case we obtain $S/V = 2100\ \text{cm}^{-1}$. In our companion article[10] we calculated the average S/V for our five samples to be 690 cm^{-1}. The difference between these two estimates is the result of high sensitivity to small variations in n_h and n_s, which are nearly equal (see Table II). In a system such as ours, where there is an inherent uncertainty in the exact composition of the surrounding liquid and its density, the use of Porod scattering to measure absolute surface area is not practical. In the companion study,[10] where the contrast was carefully calibrated via the contrast variation technique, the uncertainty in comparing relative values is significantly smaller.

One notes also in Fig. 1 a significant baseline change, 0.052 to 0.038 cm^{-1}, upon partial freezing of the sample. The baseline contribution consists of the sum of incoherent scattering, due to the presence of isotopic impurities and multiple nuclear spin states, and coherent scattering other than the Porod scattering described above. As the density change upon freezing is negligible (see Table II), the overall composition in the scattering volume is unchanged and the incoherent scattering is approximately constant. Hence, the baseline change must originate from a change in the coherent scattering. For the liquid sample, the coherent scattering comes from the liquid structure factor $S_{\text{liquid}}(q)$. For the slurry state, the contribution from $S_{\text{liquid}}(q)$ is diminished simply because the liquid fraction is cut by about one-half (the corresponding structure factor of the solid is negligible), and from this argument one might hope to use this decrease as a measure of the solid/liquid ratio. However, estimating the coherent portion of the signal for our solvents, which are largely heavy water, is quite difficult due to the effects of inelastic and multiple scattering.[21,22] Therefore, we treat the baseline as a single, q-independent, fit parameter. As can be seen in Fig. 1, this is a good approximation. The peak in $S_{\text{liquid}}(q)$ and the Bragg peaks from the crystalline state appear at much larger values of q.

Baseline changes similar to those seen in Fig. 1 are found upon partial freezing of every sample studied here. In the polymer containing samples, though, this change is often not as clearly visible due to high-q scattering from the polymer and must be extrapolated from functional fits to the data.

B. Polymer solutions and slurries

1. Polymer solutions above the hydrate formation temperature

For each of the four polymers studied in the D_2O/TDF solvent, SANS data were taken at a temperature above the hydrate formation point, 7 °C. The concentrations utilized are given in Table I. Each concentration is well below the overlap concentration, c^*; therefore we expect these data to exhibit typical single-chain scattering. Examination of the data [Fig. 2(a)] shows that in addition to this scattering there is a low-q intensity rise. We model the overall scattering as

$$I(q) = (n_p - n_s)^2 S_{\text{Beaucage}}(q) + Aq^{-2.5} + b, \tag{6}$$

where A is an amplitude to be determined from the fits, b is the background intensity, and $S_{\text{Beaucage}}(q)$ is a Debye-like structure factor for single-chain scattering,

$$S_{\text{Beaucage}}(q) = G[\exp(-q^2 R_g^2/3) + d_f \Gamma(d_f/2)/(R_g q^*)^{d_f}], \tag{7}$$

due to Beaucage.[23,24] Here, $q^* = q/[\text{erf}(kqR_g/\sqrt{6})]^3$ with $k \approx 1.06$, and $\Gamma(n)$ is the gamma function. The three fitting parameters in this structure factor allow us to extract the single-chain characteristics: polymer radius of gyration R_g, fractal dimension of the polymer coils d_f, and the Guinier prefactor G (see Table III).

For both PEO (Ref. 25) and PVP,[12] previous work has shown that these polymers exhibit ''good-solvent'' behavior in pure water at room temperature. From a knowledge of their phase behavior,[14,26,27] we can assume that no change is induced by the introduction of TDF nor by the lowering of the temperature. Therefore we can expect these two polymers to exhibit the fractal dimension predicted for a linear chain in good solvent, 5/3. In fact, Table III shows this is in

TABLE III. SANS results for polymer solutions at 7 °C.

Sample	Radius of gyration (Å)	Fractal dimension	Guinier amplitude (cm^{-1})	Amplitude for $q^{-2.5}$ power law ($\times 10^{13}\,cm^{-1}$)
PEO	80	1.9	0.41	1.3
PVP	80	1.8	0.38	4.8
PVCap	155	1.7	1.83	2.0
VIMA/VCap	70	1.7	0.35	6.9

reasonable agreement with the values obtained for all four polymers. From the good-solvent molecular-weight scaling relationships for PEO and PVP (e.g., $R_g = KM_W^m$, where K and m are empirically determined numeric values, with $m \approx 1/d_f$), we can estimate the radius of gyration from the molecular weights in Table I as, respectively, $R_g = 112$ Å and $R_g = 71$ Å. For the PVCap sample a reliable value of the molecular weight is unavailable. Using that molecular weight calculated from the Guinier amplitude [Eq. (8)] along with the molecular-weight scaling law given by Eisele and Burchard,[13] we estimate $R_g = 110$ Å. The values in Table III are in reasonable agreement with these good-solvent values, though it must be recalled that the numeric values K and m are measured in the high molecular weight limit. The VIMA/VCap copolymer also exhibits a size commensurate with its molecular weight in Table I, evidence that it too exhibits a simple random coil behavior.

For a given concentration c of a polymer, the Guinier amplitude depends on the molecular weight, with a second-order dependence on the second virial coefficient A_2 according to

$$G = (n_p - n_s)^2 (c/\rho^2)/N_A(1/M_W + 2A_2 c), \tag{8}$$

where ρ is the polymer density. [See Eq. (A3.29) from Higgins and Benoît.][20] The calculated values are as follows: PEO, 0.546 cm^{-1}; PVP, 0.491 cm^{-1}; and VIMA/VCap, 0.462 cm^{-1}. Because we have no independent measure of M_w for PVCap its value cannot be calculated. As has been noted by previous workers,[28] the observed Guinier amplitudes for polymers in aqueous systems are systematically too small for their molecular weight. As can be seen in comparing these calculated values with those in Table III, this is also the case here.

The low-q rise in scattering which we observe for each of our four polymer solutions is indicative of large structures in the solutions. Such features are a common observation for polymers in aqueous solution, and there is still some debate as to whether they are characteristic of such systems[29] or merely the consequence of contaminants. For PEO, this has been extensively studied. Recent work[25,30] suggests that impurities in the water play a key role in the aggregation. In contrast, for PVP in highly-purified water, aggregation is observed in the semidilute regime, and the amount of aggregation could be reproducibly varied by pressure experiments. Hence, it was concluded that aggregation is intrinsic to that system.[12] Light scattering studies of VIMA/VCap show that aggregates occur, even in highly purified water, well into the dilute regime for that copolymer. Therefore, the low-q scattering we observe here for the hydrate-inhibitor polymers may be due to an aggregation that is intrinsic to those materials. We have chosen to model these aggregates with a $q^{-2.5}$ power law form, which would imply a fractal structure more compact than that of the polymer chains themselves and without a sharp interface with the surrounding media. This is consistent with the results from Sun and King.[12] The resulting amplitudes are given in Table III.

We conclude from these studies that all four polymers exhibit similar characteristics, reflecting a polymer conformation typical of a swollen linear-chain polymer in a good solvent. There is no evidence of an unusual effect on the polymer conformation due to the solvated hydrate-forming molecule TDF. The low-q scattering, although not part of the linear-chain scattering, is not particularly unusual for water-soluble polymers. Comparison of PEO with the other polymers suggests that the hydrate inhibitors may have an elevated level of this low-q scattering. This may be indicative of an important interaction for hydrate inhibition: our companion article[10] finds that self-aggregation of the polymer occurs on the hydrate crystal surface. In light of these results, it is interesting to note that in the propane/D_2O system discussed below, we find an enhancement in low-q scattering beyond that seen in the TDF/D_2O system. Thus, supramolecular association may be a key feature of hydrate inhibitor polymers.

2. Polymer solutions below hydrate formation temperature, slurry scattering

a. PEO. In Fig. 2(b). we show the SANS data for the PEO sample in the slurry state. As noted for the polymer-free slurry (Fig. 1), there is a significant low-q scattering associated with the Porod scattering. At higher q-values, the polymer scattering is dominant. If the polymer does not interact with the hydrate crystals, we expect the scattering to consist of a linear combination of Porod and polymer solution scattering. The dashed line in Fig. 2(b) is the result of addition of a Porod term to the (scaled) fit in Fig. 2(a). The Porod amplitude as well as the overall background were allowed to vary, but the solution scattering was simply scaled for the increase in concentration due to exclusion of the polymer into the remaining 0.49 fraction of the sample[10] which is still liquid. For this scaling we utilized Eq. (8), where only the concentration in the numerator changes (the total mass of the polymer in our scattering volume is unchanged, so the value of c in the denominator is unaltered). The resulting scaling constant is 0.64. As is evident, this model closely approximates the observed scattering. As a further test of the robustness of this fit, we allowed the Porod and the polymer scattering variables to simultaneously vary, giving the best-fit result shown by the solid line in Fig. 2(b). The most notable change in the polymer scattering is a shift to a smaller radius of gyration, 62 Å. This reduction of characteristic length with increasing concentration is well-known.[31] Utilizing D_2O as a solvent, we have measured this effect for our PEO sample and find that the ratio in size when doubling the concentration is 0.77, essentially identical to the size change obtained by the fitting procedure described here. We conclude from these results that the PEO in coexistence with the

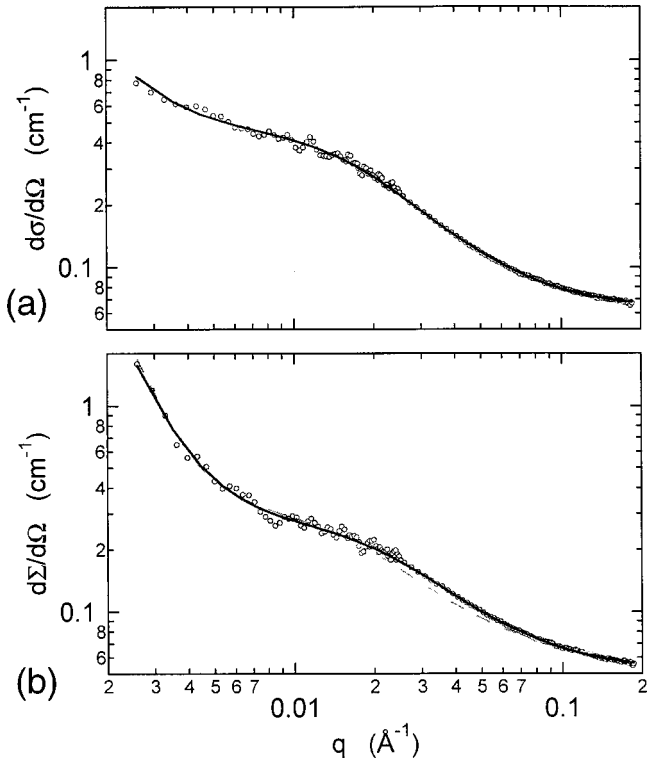

FIG. 2. Differential scattering cross-section for PEO in TDF/D_2O solvent. (a) Polymer scattering from solution, 7 °C. Solid line is best fit to Eq. (6). (b) Crystal-plus-liquid slurry scattering at 2.5 °C. The PEO conformation is nearly unaltered as evidenced by the fit of the dashed curve, a linear combination of Porod scattering from the hydrate crystal surfaces, and polymer-solution scattering [curve (a) scaled for the reduction of the liquid volume]. The small change in polymer radius of gyration, solid line, is that predicted for the increased concentration of polymer in solution (see text).

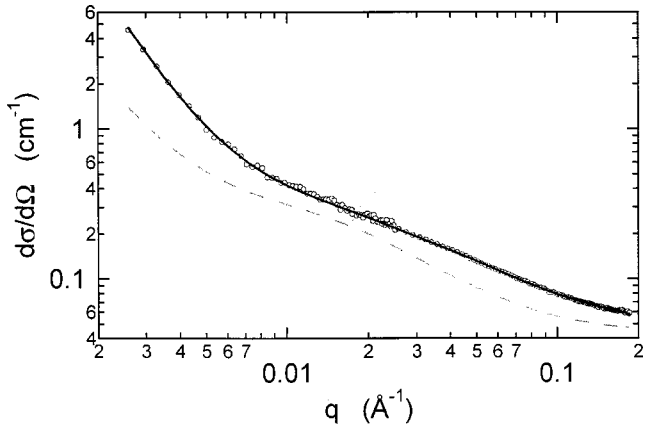

FIG. 3. Differential scattering cross-section for PVP in TDF/D_2O crystal-plus-liquid slurry at 3.0 °C. Dashed line, linear combination of Porod scattering from the hydrate crystal surfaces, and polymer-solution scattering (scaled polymer scattering from solution at 7 °C), is not a reasonable model. Significant excess scattering is present due to polymer adsorbed on the hydrate crystal surfaces. Solid line, free fit including the Beaucage, Porod, and $q^{-2.5}$ structure factors, gives unphysical polymer conformation values.

hydrate crystals has the same conformation as a polymer solution at double (0.0113 g/cc) the starting concentration. There is no evidence of an adsorbed layer.

The Porod amplitude is less readily interpreted. As can be seen by substituting the values from Table II into Eq. (5), our fitted values for the Porod amplitude seemingly imply a significant increase in surface area over the polymer free case. However, optical microscopy shows that the resulting crystals are essentially unaltered by the presence of PEO. As we noted above, in a situation such as this, where the scattering contrast between the solution and the crystal is nearly zero, an accurate calculation of the surface area is not possible. Based upon optical measurements, we believe the surface-to-volume ratio is unchanged.

b. PVP. In Fig. 3, we show the slurry-state scattering from the PVP sample. One again notes a significant low-q scattering. Comparison with Fig. 2(b) shows that the amplitude is significantly enhanced over that from the PEO sample. At higher q-values, there is also a higher level of scattering than for PEO. A linear combination of Porod and polymer-solution scattering is unable to account for these data, as shown by the dashed line, which is the scaled (by 0.75 in this case) intensity from the polymer solution. Clearly there is an excess of scattering at all q-values, not only in the Porod regime. We can fit the scattering data by allowing all the terms in the Porod and polymer solution scattering models to vary. The resulting solid line well describes the data. However, the polymer conformation one obtains is unrealistic, including a fractal dimension approaching unity due to the slow decline of the intensity at higher q-values. In our companion article,[10] we described the total scattering as a combination of three structure factors:

$$I(q)=(n_h-n_s)^2S_{gg}(q)-2(n_h-n_s)(n_p-n_s)S_{pg}(q)+(n_p-n_s)^2S_{pp}(q). \quad (9)$$

Through use of contrast variation techniques we then obtained independent values for each of the structure factors. The S_{gg} structure factor corresponds to that of Porod scattering, and for PVP it is increased over the Porod scattering in a polymer-free slurry. This is consistent with an increased surface area due to the polymer-induced change in the aspect ratio for kinetically-inhibited hydrate crystals. The other two structure factors describe the polymer scattering. The last term in Eq. (9) is the most significant and consists of two parts. One part is simply the scattering from polymer remaining in solution [Eq. (9) is derived in Auvray and Cotton[32] for the case where no polymer remains in solution]. Subtracting this solvated-polymer scattering, we are left with the scattering from adsorbed polymer. This scattering contributes across the entire q-range, and we ascribe it to two parts. At low-q, we utilize a step function, and for PVP we find that the contribution to the intensity from this term is larger than that of the Porod scattering. At higher values of q, we describe the scattering through a ''blob'' scattering structure factor, characteristic of the semidilute concentrations within the adsorbed layer. Thus through use of these structure factors and Eq. (9), we account for the complete scattering profile observed in Fig. 3.

c. PVCap and VIMA/VCaP. The slurry scattering for PVCap is shown in Fig. 4 and that for VIMA/VCap in Fig. 5. Note that the low-q scattering amplitudes here are even larger than that for PVP. At higher q-values, a quantitative comparison with the scaled liquid-state polymer scattering is

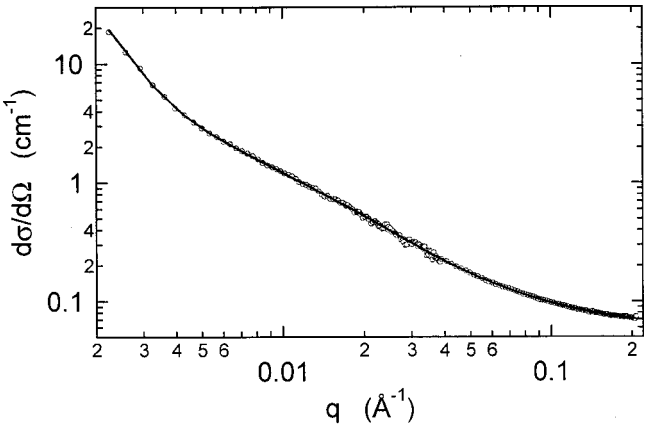

FIG. 4. Differential scattering cross-section for PVCap in TDF/D_2O crystal-plus-liquid slurry at 3.3 °C. Increased low-q scattering compared to that for PVP suggests increased polymer adsorption onto hydrate crystal. Solid line, free-fit as for Fig. 3.

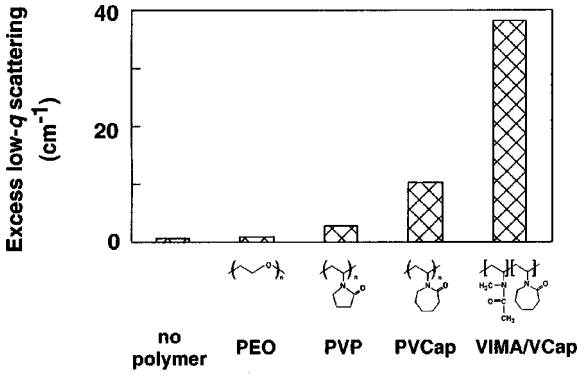

FIG. 6. Excess low-q scattering, defined as the difference between the intensities at $q=0.0025$ Å^{-1} for crystal-plus-liquid slurry minus polymer solution. The excess scattering increases as the effectiveness of the additive increases from PEO (a noninhibitor polymer) to VIMA/VCap (the most active inhibitor studied here). This excess scattering is attributed to the amount of polymer in the inhibitor layer, suggesting that increased polymer adsorption is a key feature of the inhibitor mechanism.

hampered because we do not have sufficiently accurate second virial coefficients, but qualitative comparison suggests that both curves exhibit excess scattering similar to that for PVP. Thus, we interpret the scattering for these two cases as similar to that for PVP, indicative of polymer adsorbed to the hydrate crystal surface.

d. Low-q Scattering Amplitudes and Inhibitor Effectiveness. As we note in the descriptions above, there is a progression towards greater low-q scattering as we proceed through our five slurry samples, one polymer-free and four polymer-containing. We can quantify this by plotting the difference in scattering between the 2.5 °C data and that at 7 °C for our lowest q-value, 0.0025 Å^{-1}. These amplitudes are shown in Fig. 6. In this plot the effectiveness of the hydrate inhibitor polymer increases toward the right, with VIMA/VCap being the most effective.

The difference in behavior between the three (PVP, PVCap and VIMA/VCap) inhibitor-containing slurries and the two (polymer-free and PEO) noninhibitor ones comes from two sources, as we discuss in our companion article.[10] There is an increased surface area associated with the change in aspect ratio for the inhibitor-modified crystals, and there is a significant contribution to the low-q intensity from the polymer on the hydrate surface. However, of greater interest here is the systematic intensity increase as the effectiveness of the inhibitor increases. This could help illuminate the mechanism of hydrate inhibitor function.

Examination of the structure factors contributing to the intensity described by Eq. (9) suggests that the values in Fig. 6 provide an estimate of the amount of polymer adsorbed to the hydrate crystal surface. In our companion article[10] we model the adsorbed PVP polymer layer by assuming it forms a layer consisting of a volume fraction ϕ of polymer in a layer thickness of h. The relevant polymer structure factor is

$$S_{pp}^{\text{step}} = 4\pi(S/V)\phi^2(1-\cos qh)/q^4. \tag{10}$$

where S/V is the surface/volume occupied by the polymer (for PVP the ratio of S/V to S/V-total is about 0.02). Using the values determined for PVP ($h=550$ Å and $(S/V)\phi^2 = 0.392\,\text{cm}^{-1}$, and S/V-total$=5000\,\text{cm}^{-1}$) along with the scattering length densities from Table II, we find that for PVP over half of the low-q intensity comes from the adsorbed polymer layer. This high degree of sensitivity to a small amount of polymer is achieved through use of hydrogenated polymer in this otherwise deuterated system.

To explain our observation that there is an enhancement in the low-q intensity for the more effective inhibitors, we can appeal to two scenarios. In scenario one we imagine that an increase in surface area is the cause. This mainly increases the S_{gg} structure factor, but there is a corresponding increase in S_{PP} as indicated by Eq. (10). Assuming that the fraction of the surface (0.02) occupied by polymer remains constant, we calculate that the observed fifteen-fold increase in low-q scattering for VIMA/VCap over that for PVP (Fig. 6) implies a more than thirty-fold increase in surface area. This considerably larger surface area would give, for spherical crystals, an average crystal radius of about 0.1 μm. Mass balance constraints demand a considerably larger number of crystals, a more than 10^4 increase for spherical crystals. Increased number and reduced crystal size might, indeed, be a

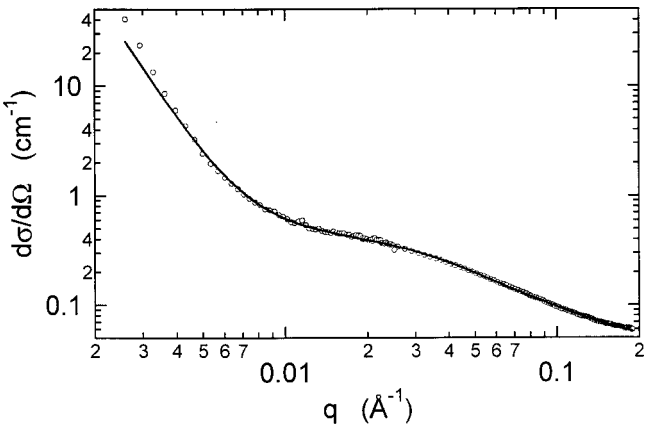

FIG. 5. Differential scattering cross-section for VIMA/VCap in TDF/D_2O crystal-plus-liquid slurry at 2.5 °C. Increased low-q scattering compared to that for PVP and PVCap suggests increased polymer adsorption onto the hydrate crystal. Solid line, free-fit as for Fig. 3.

feature of a more effective hydrate inhibitor, but it's difficult to envision how this occurs for the same amount of polymer adsorbed to the surface. If we accept this scenario, we are still left with a mystery as to how it is achieved.

In scenario two, we attribute the increased intensity to increased polymer on the surface. To account for the same fifteen-fold intensity increase requires that the prefactor, $(S/V)\phi^2$, increase more than twenty-fold. From our previous discussion, it should be apparent that this could be due to an increased area of coverage (>0.02) or a higher volume fraction of polymer. We calculate that for PVP the concentration within the layer is already $\approx 2.5c^*$; therefore, it is more reasonable to suppose that more of the surface is covered.

In our companion article, we argue that polymer adsorbed to the surface acts as a growth arrestor and that this is likely an important mechanism for the activity of a polymeric gas–hydrate inhibitor. From consideration of a step-flow growth model, we suggest that the pinning of steps will slow growth by a factor of $1-2r^*/l$, where r^* is the critical nucleus radius on the surface and l is the spacing between pinning sites. We estimate this spacing as ~2300 Å for PVP. This would decrease significantly if more of the surface were covered thus further slowing crystal growth. Therefore, we suggest that the increased amplitude is, at least partly, due to greater surface coverage by the inhibitor and a corresponding slowing of the crystal growth. Likely, the increased polymer coverage would also result in an increased surface area due to the growth inhibition.

One further consideration that should be mentioned is that increasing the thickness of the polymer layer [for constant $(S/V)\phi^2$] cannot account for the intensity increase. This is clear from Eq. (10) which shows that as h increases, the peak in the intensity moves to a lower q, thus lowering the intensity within our experimental q-range. A thinner layer appreciably decreases the low-q scattering as is also evident from Eq. (10). We mention this, because we suppose that the layer thickness may be proportional to R_g. This would then suggest that in comparing polymers of significantly lower molecular weight with those measured here, one might observe a diminished low-q intensity. In this instance, a complete contrast variation study would be needed to determine the extent of the polymer layer coverage.

3. Propane/D_2O system at elevated pressure

The experiments described above were all conducted using a fully-miscible hydrate forming molecule, but there is some question whether such a system duplicates the full range of possible polymeric hydrate inhibitor behavior. For example, it has been suggested[5] that kinetic inhibitors may affect nucleation behavior, thus acting upon the fluid components prior to actual crystallization. As we note above, there is little evidence for this in the case of the TDF/D_2O system, but, clearly the important commercial use of hydrate inhibitor polymers is for gas-plus-water systems. To investigate this, we studied the polymer conformation in a uniform fluid consisting of D_2O saturated with a hydrate forming gas, propane. Through temperature variation, we can take the system from the gas–liquid stability region to the hydrate–gas–liquid region. Owing to the well known tendency for gas hydrates to form at the gas–water interface rather than throughout the bulk,[16] making a uniform crystal–liquid slurry under such conditions would be a very difficult task. Because hydrate crystals do not easily nucleate at the small subcoolings studied here, we are able to measure the sample in the fluid state during our experiments.

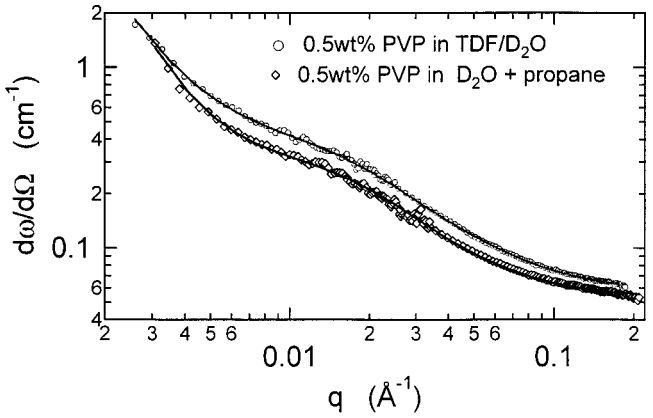

FIG. 7. Differential scattering cross-section for PVP in two hydrate-forming solvents. Circles, data from TDF/D_2O at ambient pressure and 7 °C. The solid line is the best fit to Eq. (6). Diamonds, data from propane/D_2O at 655 kPa and 6.7 °C. Solid line is a best fit to Eq. (6), replacing the $q^{-2.5}$ power-law with q^{-3}. A more compact nature of the aggregates is evident from the required change in power law. Also, the lower level of scattering across most of the q-range suggests that more of the polymer is bound in the aggregates. The data at 20 °C, 10 °C, and 3.7 °C are essentially identical.

Figure 7 shows a comparison between SANS data taken for PVP in a TDF/D_2O solvent at 7 °C and in a propane/D_2O solvent system at the same temperature. In the latter case, the system is in the hydrate–gas–liquid stability range. The solid line for the TDF/D_2O solvent is the best fit to Eq. (6), as previously discussed. The solid line for the propane D_2O solvent is similar to Eq. (6), but we are unable to fit the low-q scattering with a power law of $q^{-2.5}$. Instead, a power law of q^{-3} is used. The resulting Beaucage fit parameters for PVP in the propane/D_2O solvent are: $R_g = 75$ Å, fractal dimension $= 1.96$, and Guinier amplitude $= 0.286\ \mathrm{cm}^{-1}$. As the similar shapes of the scattering profiles in Fig. 7 suggest, these values show that the single-chain conformation of the polymer is little changed from that in the TDF/D_2O solvent. Comparison with the values in Table III shows there is a slight shift toward a fractal dimension more similar to that of a poor solvent (II) and a Guinier amplitude that is reduced further from that predicted from Eq. (8) (the contrast change due to the change in solvent is insufficient to account for this difference).

The decreased Guinier amplitude and enhanced low-q scattering may indicate that more of the polymer participates in forming aggregates. As evidenced by the -3 power law at low-q, the aggregates here are more compact that the aggregates previously described. Thus, it is possible that the polymer may associate with the hydrate-forming gas in a different manner than with solvated TDF. However, changing the temperature causes no significant change in the scattering over the range of our investigations. It has been found that water structuring induced by hydrate-forming gases can persist, on a local scale, above the liquid–hydrate–gas stability

range.[33] Perhaps these associations for the polymer–propane–D_2O system are similar and persist to above the maximum temperature we studied, 20 °C. It is possible that these aggregates play a role in the gas–hydrate inhibition function. For example, if they act as gas sinks, isolating the gas from the water, they would, in effect, reduce the local supersaturation and thus impede nucleation.

IV. CONCLUSIONS

In conclusion, we have presented SANS data for four polymers in hydrate-forming liquids both above and below temperatures where the hydrates are stable. In the temperature range when hydrate crystals coexist with a liquid, we find that those polymers that act as kinetic hydrate inhibitors change their conformation. This conformation change is believed to signal an adsorbed polymer layer on the hydrate crystal surface. PEO, a noninhibitor polymer, does not exhibit this excess scattering signal. The SANS in that case can be quantitatively described as the sum of Porod scattering from crystal surfaces and scattering from solvated polymer. In a companion article,[10] we used the SANS contrast variation technique to study the adsorbed layer for one inhibitor, PVP. If we assume that a similar interpretation is applicable to the other two inhibitor polymers studied here, the majority of the low-q scattering will come from adsorbed polymer. This allows us to utilize the low-q scattering as a measure of the inhibitor adsorption and we find a correlation between effectiveness and the amplitude of the scattering. This implies that a principle mechanism of hydrate kinetic suppression involves surface adsorption onto growing crystals with attendant slowing of the growth.

The above results were obtained for a soluble-molecule hydrate forming system, TDF/D_2O. In the case of a gas-molecule hydrate forming system, propane–D_2O, we investigated the polymer conformation in the absence of hydrate crystals. The polymer conformation is altered from that in the TDF/D_2O solvent. The most significant change is an anomalous low-q scattering, indicative of the formation of large, compact aggregates in the fluid phase. We suggest these could signal an association between the hydrate-forming components and the polymer, which might act to alter the nucleation behavior (a mechanism suggested by Lederhos *et al.*).[5] Our results in this system are rather limited; clearly, further neutron scattering studies of this system are warranted.

ACKNOWLEDGMENTS

We would like to thank the following: Karla Colle for sample syntheses, John Huang for helpful suggestions on neutron scattering, Scott Milner for conversations regarding polymer adsorption and scattering theory, and Larry Talley and John Longo for discussions of hydrate inhibitor function. We also acknowledge the NIST Center for Neutron Research and Exxon PRT for providing beamtime and help during the measurements.

[1] D. W. Davidson, in *Water: A Comprehensive Treatise*, edited by F. Franks (Plenum, New York, 1973), Vol. 2, pp. 115-225.
[2] K. A. Kvenvolden, in *International Conference on Natural Gas Hydrates*, edited by E. D. Sloan Jr., J. Happel, and M. A. Hnatow, N.Y. Acad. Sci. **715**, 232 (1994).
[3] E. D. Sloan, Jr., *Clathrate Hydrates of Natural Gases* (Marcel Dekker, New York, 1990).
[4] E. D. Sloan, Jr., J. Pet. Technol. **43**, 1414 (1991).
[5] J. P. Lederhos, J. P. Long, A. Sum, R. L. Christiansen, and E. D. Sloan, Jr., Chem. Eng. Sci. **51**, 1221 (1996).
[6] R. L. Christiansen, Y. Du, J. P. Lederhos, J. P. Long, V. Panchalingan, E. D. Sloan Jr., and A. K. W. Sum, Patent WO 9532356 (1995).
[7] T. Y. Makogon, R. Larsen, C. A. Knight, and E. D. Sloan, Jr., J. Cryst. Growth **179**, 258 (1997).
[8] R. Larsen, C. A. Knight, and E. D. Sloan, Jr., Fluid Phase Equilibria **150-151**, 353 (1998).
[9] E. D. Sloan, Jr., S. Subramanian, P. N. Matthews, J. P. Lederhos, and A. A. Kokhar, Ind. Eng. Chem. Res. **37**, 3124 (1998).
[10] J. Hutter, H. E. King, Jr., and L. Y. Min, Macromolecules (in press).
[11] E. Smelik (personal communication).
[12] T. Sun and H. E. King, Jr., Macromolecules **29**, 3175 (1995).
[13] M. Eisele and W. Burchard, Makromol. Chem. **191**, 169 (1990).
[14] E. Nordmeier and M. D. Lechner, Macromolecules **24**, 2529 (1991).
[15] H. J. M. Hanley, G. J. Meyers, J. W. White, and E. D. Sloan, Jr., Int. J. Thermophys. **10**, 903 (1989).
[16] E. A. Smelik and H. E. King, Jr., Am. Mineral. **82**, 88 (1997).
[17] A. Harmens and E. D. Sloan, Jr., Can. J. Chem. Eng. **68**, 151 (1990).
[18] R. Kobayashi and D. L. Zatz, Ind. Eng. Chem. Res. **45**, 440 (1953).
[19] NIST, *NG3 and NG7 30-Meter SANS Instruments Data Acquisition and Reduction Manual* (National Institute of Standards and Technology, Center for Neutron Research, Gaithersburg, MD, 1999).
[20] J. S. Higgins and H. C. Benoît, *Polymers and Neutron Scattering* (Oxford University Press, Oxford, 1994).
[21] R. P. May, K. Ibel, and J. Haas, J. Appl. Crystallogr. **15**, 15 (1982).
[22] A. K. Soper, Physica B **136**, 322 (1986).
[23] G. Beaucage, J. Appl. Crystallogr. **29**, 134 (1996).
[24] G. Beaucage, J. Appl. Crystallogr. **28**, 717 (1995).
[25] K. Devanand and J. C. Selser, Macromolecules **24**, 5943 (1991).
[26] T. Sun and H. E. King, Jr., Phys. Rev. E **54**, 2696 (1996).
[27] T. Sun and H. E. King, Jr., Macromolecules **31**, 6383 (1998).
[28] A. Poppe, L. Willner, J. Allgaier, J. Stellbrink, and D. Richter, Macromolecules **30**, 7462 (1997).
[29] P. G. de Gennes, C.R. Acad. Sci., Ser. II: Mec. Phys., Chim., Sci. Terre Univers **313**, 1117 (1991).
[30] K. Devanand and J. C. Selser, Nature (London) **343**, 739 (1990).
[31] P. Wiltzius, H. R. Haller, D. S. Cannell, and D. W. Schaefer, Phys. Rev. Lett. **51**, 1183 (1983).
[32] L. Auvray and J. P. Cotton, Macromolecules **20**, 202 (1987).
[33] F. Fleyfel, K. Y. Song, A. Kook, R. Martin, and R. Kobayashi, J. Phys. Chem. **97**, 6722 (1993).
[34] S. W. Lovsey, *Theory of Neutron Scattering from Condensed Matter* (Oxford University Press, Oxford, 1984).
[35] O. Kiyohara and G. C. Benson, International Data Series, Ser. B: Thermodynamic Properties of Aqueous Organic Systems. 2a. Excess Volume (Engineering Sciences Data Unit, 1979).
[36] P. Molyneux, *Water-Soluble Synthetic Polymers: Properties and Behavior* (CRC, Boca Raton, 1983).